Multi-Input Single-Inductor MPPT Regulator with Sliding-Mode Controller

by

Yu Geng

A Thesis Presented in Partial Fulfillment
of the Requirements for the Degree
Master of Science

Approved May 2017 by the
Graduate Supervisory Committee:

Sayfe Kiaei, Chair
Bertan Bakkaloglu
Jennifer Kitchen

ARIZONA STATE UNIVERSITY

August 2017

ABSTRACT

A Multi-input single inductor dual-output Boost based architecture for Multi-junction PV energy harvesting source is presented. The system works in Discontinuous Conduction Mode to achieve the independent input regulation for multi-junction PV source. A dual-output path is implemented to regulate the output at 3 V as well as store the extra energy at light load condition. The dual-loop based sliding-mode MPPT for multi-junction PV is proposed to speed up the system response time for prompt irradiation change as well as maximize MPPT efficiency. The whole system achieves peak efficiency of 83% and MPPT efficiency of 95%. The whole system is designed, simulated in Cadence and implemented in PCB platform.

TABLE OF CONTENTS

Page

LIST OF TABLES

Table Page

LIST OF FIGURES

Figure Page

Chapter 1

INTRODUCTION

1.1 Multi-junction PV

Green power becomes a really hot topic in the background of global warming. Photovoltaic (PV) as a good alternate for the both indoor and outdoor application is widely used in our daily life. Depending on the bandgap of the material used, silicon based single junction solar cells utilize a fraction of the solar spectrum. The earliest research on silicon based solar cells are proposed during 1940s, which indicated that the efficiency is even lower than 1%, [1], [2]. However, the hope of higher efficiency fuel the research in this domain. Years of research have been dedicated into both the material end and application end to achieve better efficiency. In 2009, a solar cell with efficiency of 24.7% has been reported [3]. The upper efficiency limit of any PV devices will be 95% at room temperature [4]. Instead of just utilizing single junction PV device, multi-junction PV device has been studied. Multi-junction PV evolves to fetch energy from a larger energy band of the solar spectrum. As reported, idea 1, 2, 3 and 36 energy gap cells have efficiencies of 37, 50, 56 and 72%, respectively [5]. And the Shockley and Queisser limit of such a multi-junction device is about 86.8% [6]. Thus, the multi-junction PV device is attractive to be used as an alternative to standard single junction device.

High Efficiency and high power density are always the key factors in the power system consideration. To extract the energy from any PV device, the load need to be modulated to match the PV input impedance for maximum power extraction. The power output from the solar cells vary with temperature, illumination and the electric load connected with it.

Therefore, maximum power point tracking (MPPT) is almost an indispensable part of a high power density delivery solar cell system. More new strategies and techniques are required for the load demanding and better power management. Vary in the complexity, sensor required, convergence time, efficiency, implementation and platform, the methods are proposed and studied. Among all the methods, perturb and observe method is the most popular method which has been used. From Figure 1, the inverse correlation between current and voltage can be seen. Thus, there is one peak power point when we multiply the current and voltage. By detecting the power change after every perturbation, we can achieve the maximum power tracking.

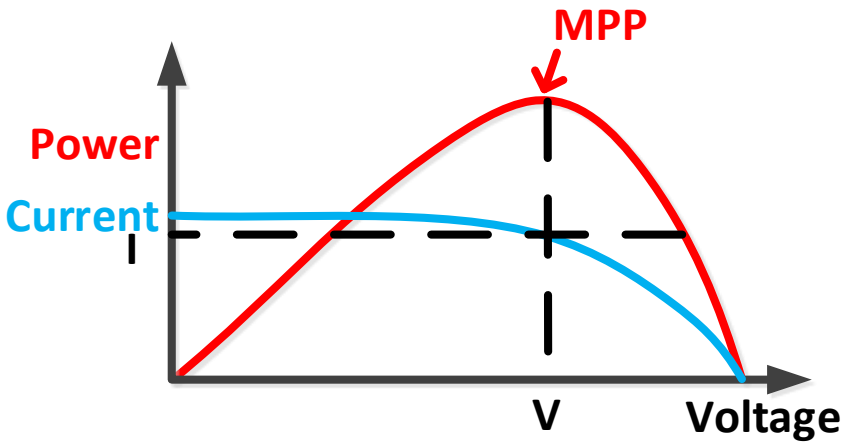

Figure 1. Multi-junction Power Management System

Usually solar cells in a multi-junction structure are interconnected in series to form a string, and multiple strings are connected in parallel to form a panel [7]. As shown in the Figure 2, the maximum power points for multi-junction vary in voltage and current. Each junction performs as isolated PV source. Thus, the challenge for extracting the power from multi-junction devices is to tract the maximum power point simultaneously from multi input sources.

Since the maximum power points for multi-junction vary from one to another. Therefore, simply adding multi-junction in parallel fashion or in series fashion will limit the current or voltage, which leads to the significant mismatch between exact maximum power point and the operating point in each multi-junction layer. Consequently, multi converters and controllers are both necessary to regulate the MPP from multi-junction PV devices. Furthermore, voltage regulation, high end to end efficiency should also be achieved [8]-[9]. Meanwhile, people contribute significant effort in achieving high efficiency in PV extracting converters. However, the total efficiency is the also affected by the MPP efficiency which depends on the steady state and transient performance [10], which brings more challenges to the designer in the application end.

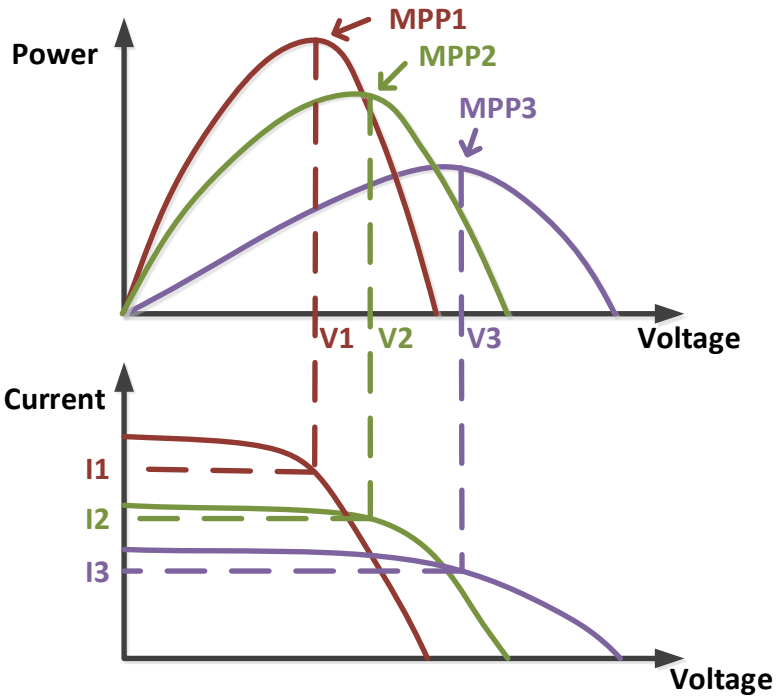

Figure 2. Multi-junction PV I-V Curve

1.2 Prior Work Limitations

Several previous studies might become good candidates as the energy extracting converter for multi-junction PV devices. Multi channels parallel dc-dc converter is easy to implement with the penalty of losing current phase alignment [11]. Interleaved Boost converter solved the conduction alignment issue with multi identical power stage components [12]. Single inductor sharing structure with time domain Hill Climbing MPPT achieves the phase alignment with less power stage components, while the control strategy is not able to handle the prompt radiation variation [10]. Sliding mode concept is introduced into MPPT to speed up the system response to the sudden change [13]-[18]. Predetermined two dimensional sliding mode MPPT is able to speed up the MPPT convergence around the two dimensional sliding surface. However, it requires offline PV characterization for one specific condition and can not handle wide environment range [17]. P&O based voltage domain sliding-mode MPPT improves system response time to the sudden illumination change along the voltage domain sliding surface. However, the output voltage is not regulated in this work, and multi MPPT controllers are required to modulate all PV inputs [18].

1.3 Highlight of This Works Contribution

In this paper, a more efficiency and low cost multi-input single inductor dual-output (MISIDO) converter is proposed for multi-input energy harvesting application. As is shown in Figure 3, the single stage structure shares inductor to extract maximum power from multi energy harvesting sources in top-level. Compared with the classic two stages cascade MPPT circuit, output regulation is achieved by reusing the same Boost MPPT stage in this work, which means that one stage power loss is reduced in operation.

Furthermore, it can store the extra energy in the battery for future use at light load condition instead of wasting that part of energy. Last but foremost, to improve the transient response to the irradiation for multi-junction PV devices, a novel sliding mode based multi-input sharing MPPT technique is presented within proposed multi-input sharing inductor structure operating in discontinuous conduction mode (DCM).

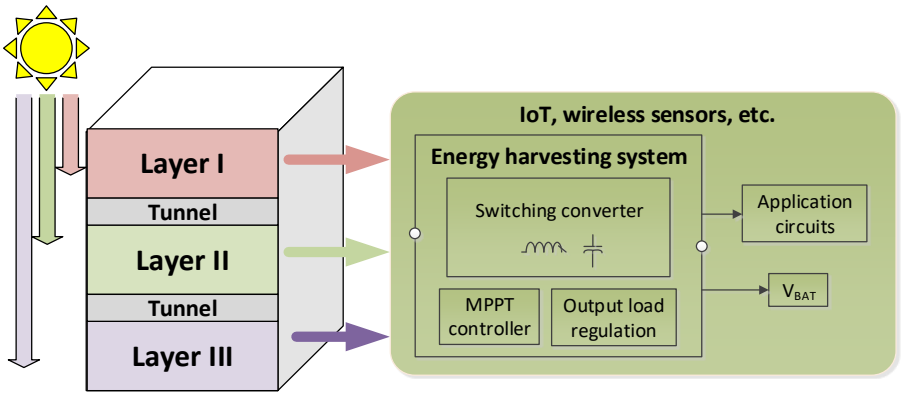

Figure 3. MJ-PV Power Management System

1.4 Thesis Organization

This thesis is organized in the following manner. Fundamental knowledge regarding PV energy harvesting and Boost regulation are discussed in Chapter 2. The details of proposed architecture and control strategy are presented in Chapter 3. Sliding mode based algorithm, stability analysis and implementation are presented in Chapter 4. Chapter 5 presents the experiment results and Chapter 6 concludes our research effort.

CHAPTER 2

FUNDAMENTALS IN PV ENERGY HARVESTING

2.1 Photovoltaic Cells

The PV cell can directly converts sunlight into electricity. The voltage and current will be varied according to the load connecting at the contact of the PV. The load can be lighting systems or DC motors. Regulation converter will be required if the load voltage requirement is strict. Moreover, the current flow or the MPPT function can be achieved by using the converter. As is shown in the Figure 4, a PV cell is basically a semiconductor diode whose p-n junction is exposed to the light [19], [20]. The single-junction PV can be made by several different materials. A thin layer of silicon is connected to the metal terminal in the silicon based PV cells. The two junctions are doped to form a p-n junction. The light injected through the junction will be absorbed and the electron and hole pair will be generated. Depending on the energy of the photons, the charges will be generated and collected at the metal terminal. Then, the charges will be delivered to the load by different voltage potential [21], [22].

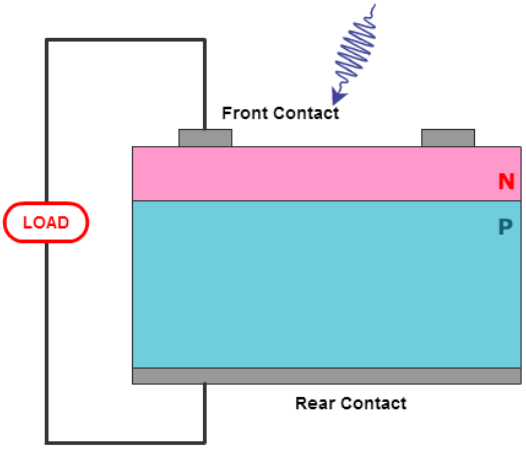

Figure 4. Single-junction PV

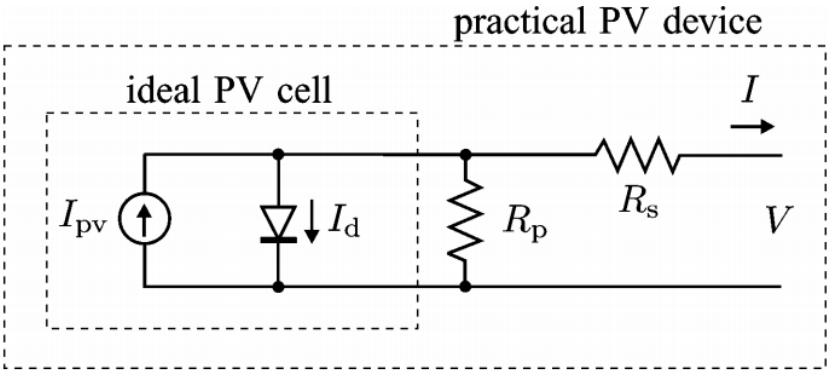

Figure 5. Single-diode Model of Idea PV Cell

Figure 5 shows the equivalent circuit of the idea PV cell. The non-linear I-V characteristic can be modelled according to the equation [23].

$$\mathrm{I} = \mathrm{I}_{PV} - \mathrm{I}_0[\mathrm{e}^{\frac{\mathrm{qV}}{\mathrm{nKT}}} - 1]$$

where IPV is the current generated by the incident light which linearly depending on the sunlight irradiation, IO is the reverse saturation or leakage current of the diode in the model, q is electron charge (i.e.1.602× 10−19 C), n is diode ideality constant, K is Boltzmann constant (i.e.1.38064852 × 10−23 J/K) and T is the kelvin temperature of the p-n junction. Fig 6 shows the plotted the I-V curve of a PV cell, where ISC stands for short circuit current, IMPP is the PV output current at its MPP operating condition, VMPP is the PV output voltage at its MPP operating condition and VOC is PV open circuit voltage.

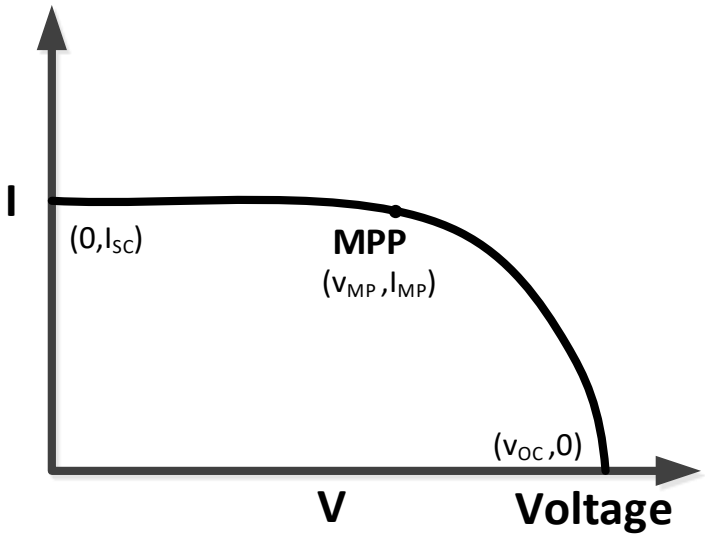

Figure 6. I-V Curve of a PV Cell

Resulting from the inverse relationship between voltage and current, the maximum power point lies in the middle of the voltage range. Furthermore, to extract the maximum power, a proper load is required to connect to the PV cells. Thus, maximum power point tracking technique is indispensable to dynamically extract maximum power from PV in practical condition.

2.2 Maximum Power Point Tracking

To extract the energy from the any active source with inner resistance, we need to tune the load properly. As shown in the Figure 7

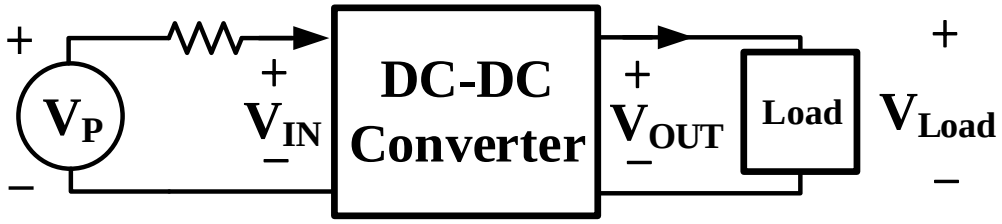

Figure 7. Impedance Matching for Energy Extraction

The relationship between V_{out} and V_{in} is modulated by the DC-DC converter duty cycle as the equation below

$$V_{out} = M(D) * V_{in}$$

Assume 100% efficiency, the output current and input current hold an inverse relationship.

$$I_{out} = \frac{1}{M(D)} * I_{in}$$

Then the input resistance of the DC-DC converter can be modulated by the duty cycle. Thus, the optimal load resistance of the energy source can be tuned by controlling the duty cycle to achieve maximum power extraction.

$$R_{out} = M(D)^2 * R_{in}$$

$$R_{in} = \frac{1}{M(D)^2} * R_{out}$$

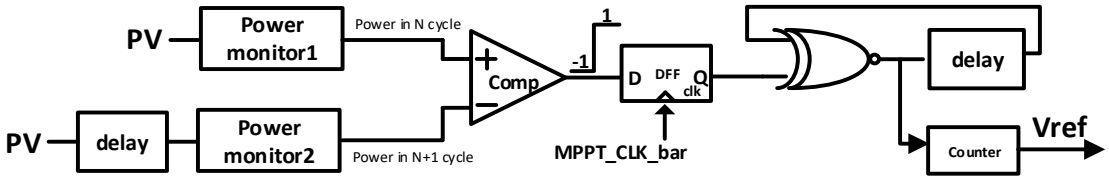

Figure 8. P&O method

Tracking the MPPT is usually an essential part in the PV application end to end system. Among all the MPPT methods, hill climbing [24]-[31] and P&O [32]–[48] is most simple to implemented. The duty ratio of the power converter is perturbed in Hill climbing method and the voltage is perturbed in the P&O method. The power information is sampled before and after perturbation. As shown in the Figure 8, power information in both cycles are compared to determine the further perturbation direction. The truth table or the XNOR gate is shown in Figure 9

XNOR Truth table

	-1	1
-1	1	-1
1	-1	1

Figure 9. XNOR Gate Truth Table

2.3 Multi-junction Energy Extraction

Because of the big difference optimal operation points among all junction, there will be significant mismatch between the optimal operation point and the real operation point if we simply parallel all junction output or put them in series as Figure 10

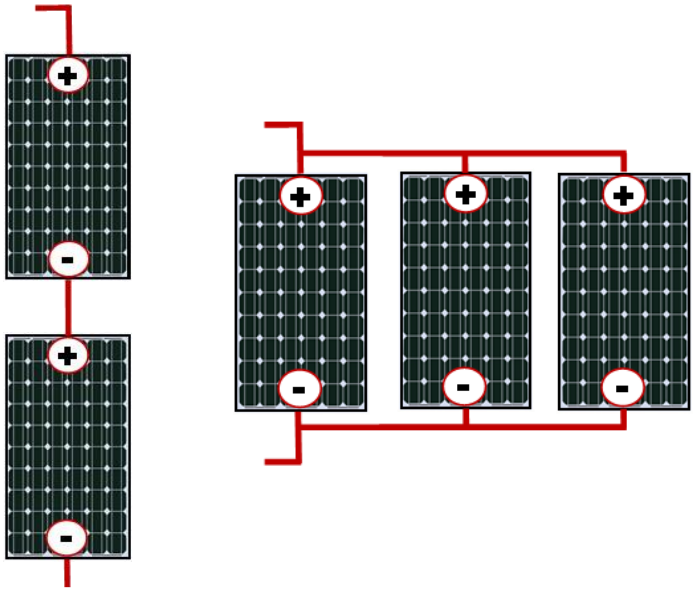

Figure 10. PV Junctions in Parallel or in Series

Thus, a DC-DC converter is required here to match the different impedance from multi-junction PV device as Figure 11

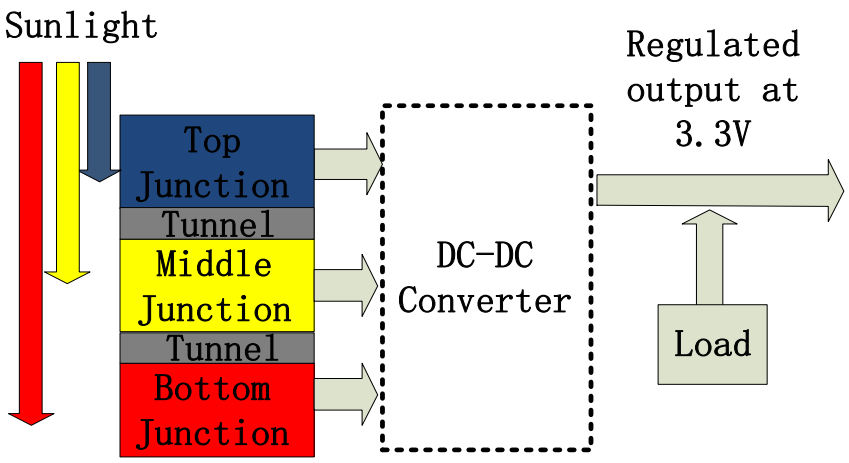

Figure 11. Utilizing DC-DC Converter for Multi-junction PV

2.4 Output Regulation

In the classic two stages design as Figure 12, first stage is responsible to track the maximum power while one more stage is required to achieve the output regulation for the load. Consequently, a lot of power stages components and controllers are required to complete the MPPT as well as the regulation function, which is not a cost-efficient option.

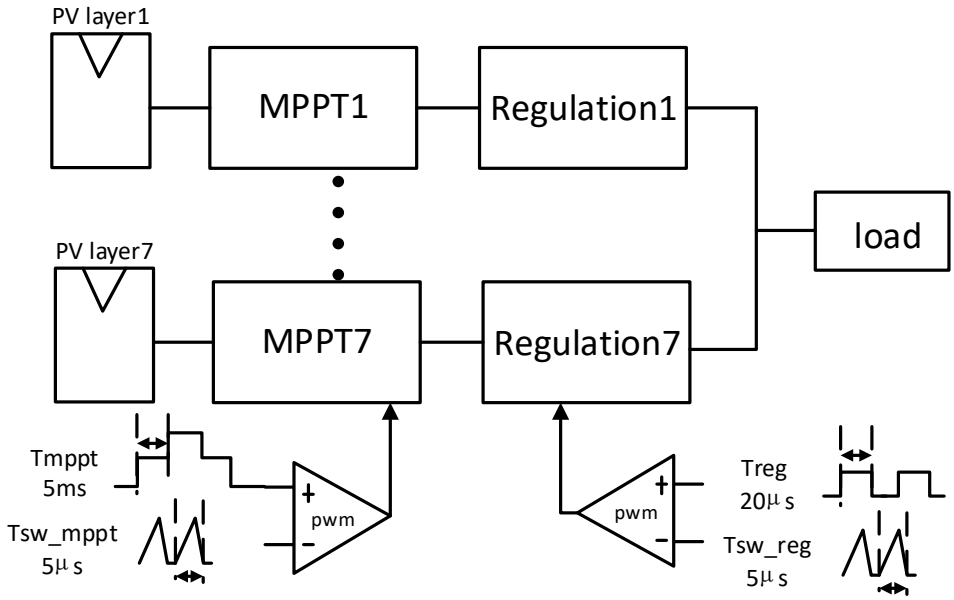

Figure 12. Cascade DC-DC for PV Application

CHAPTER 3

PROPOSED SYSTEM ARCHITECTURE AND BASIC OPERATION

3.1 Proposed System

The Top-level diagram of the proposed system is shown in Figure 13. The proposed architecture consists of three parts: Inductor sharing input multiplexer, Boost converter and dual-path output regulation. SW_1 , SW_2 , SW_3 is controlled by the input multiplexer to achieve multi-input single inductor sharing. The input selection block is an embedded finite state machine which is triggered by the clock signal from the current controller. The dual-path output regulation controller will select to deliver the inductor stored energy through one of the high side switch either SW_5 or SW_6 based on the sensed feedback load voltage. The middle Boost converter stage consists of shared inductor, SW_4 and one of the high side switches in every input selected phase.

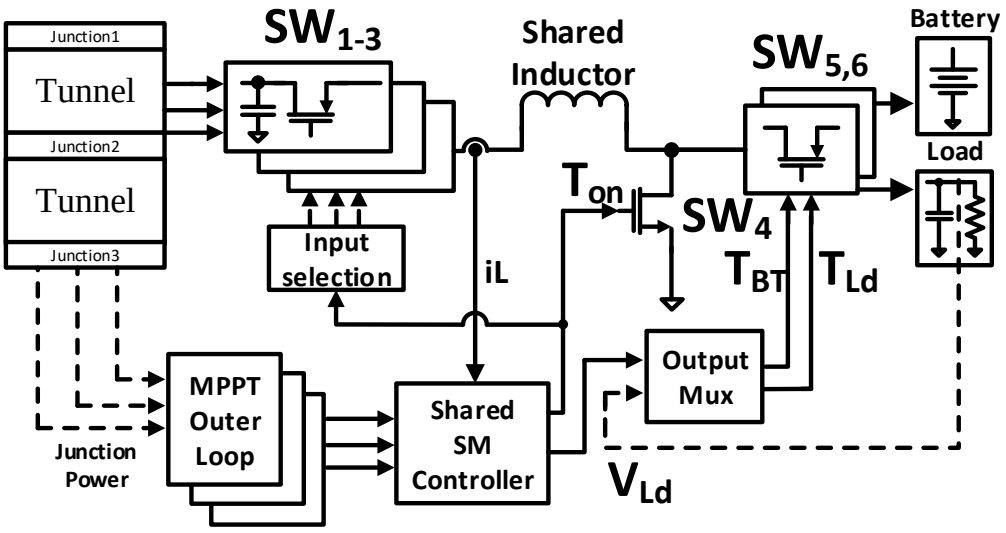

Figure 13. Top-level Diagram of the Proposed System

The controller consists of two loops: outer loop is determined by the Perturb & Observe algorithm while the inner current loop is controlled by the shared sliding-mode current controller. With the P&O algorithm, the maximum power point can be dynamically searched at a low frequency. At the meantime, the inner sliding mode current controller turns the shared inductor into an adjustable current source to speed up the current domain behavior of the whole system.

3.2 Sliding-mode MPPT Controller

The each junction operates significantly different according to irradiation, temperature and shades, which makes it difficult to predict the maximum power point. As is shown in Figure 14, sliding-mode MPPT controller consists of two loops. For the outer loop, P&O algorithm is applied to dynamically track the maximum power point for each PV junction. The power information is sensed and compared cycle by cycle to decide the perturbation direction. Thus the whole converter equivalent impedance is modulated by the duty cycle to extract the optimal power from PV input. A reference error signal is generated through error amplifier as an adaptive reference for the inner sliding mode controller. Outer loop defines the sliding surface dynamically in a much lower frequency and the inner loop speeds up the convergence speed around sliding surface. By utilizing the dual-loop technique, the perturbation step can be designed with fine step size to achieve high MPPT efficiency in steady state while the most tracking is carried out by the inner sliding mode loop to speed up the tracking performance.

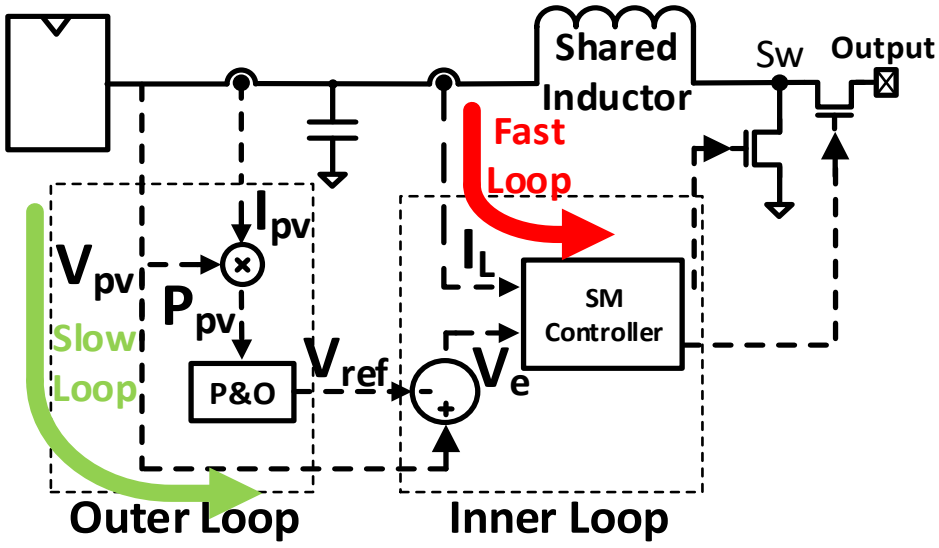

Figure 14. Dual-loop Sliding-mode MPPT

In different irradiation condition, the PV is characterized as Figure 15. Resulting from the linear dependence of the PV current on the illumination, the PV maximum power points vary significantly in current while vary insignificantly in voltage. The sharp blue line is the optimal MPPT surface for different insolation conditions.

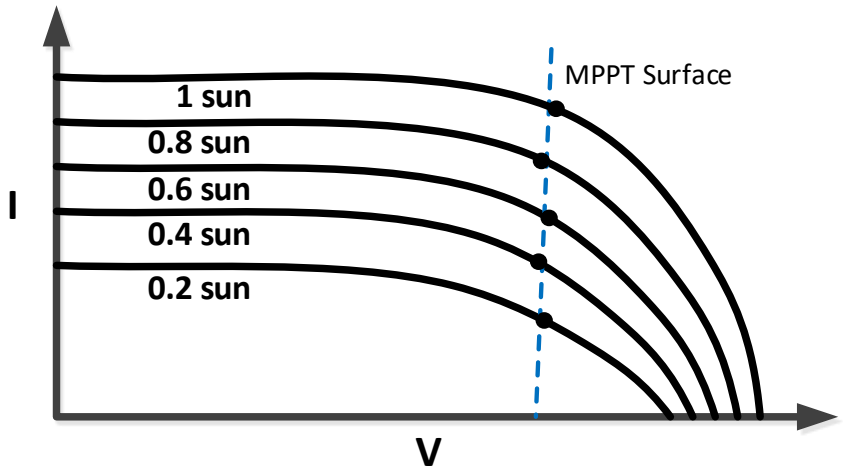

Figure 15. PV Characteristic with Different Insolations

The system slides around the adaptive surface which is generated by the P&O outer loop instead of the predetermined optimal MPPT surface which need to be characterized offline

in the idea condition. Therefore, the PV current tracking performance will be speeded up by the inner sliding mode controller while only few steps in voltage are required to complete the whole tracking behavior as the Figure 16. Consequently, high MPPT efficiency and fast irradiation response performance are both obtained with fine perturbation step in the P&O outer loop and sliding mode inner loop.

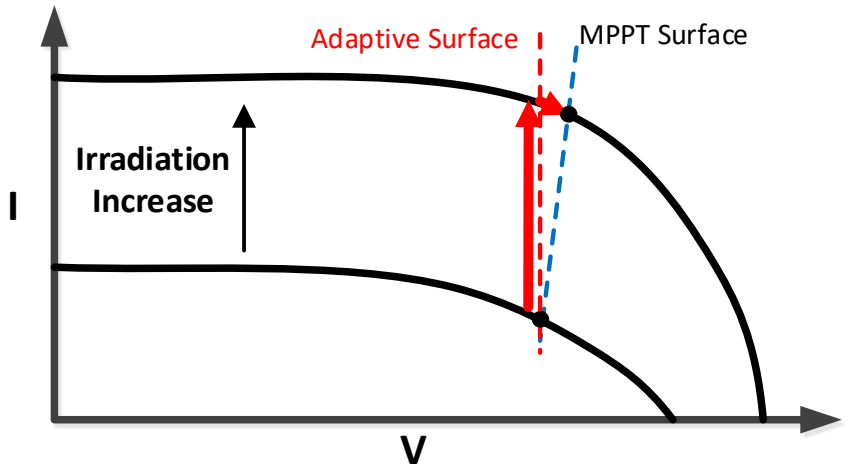

Figure 16. Sliding-mode MPPT Tracking Behavior

3.3 Input Multiplexer Sharing Single Inductor

Multi-junction PV inputs play as multiple supplies to deliver the energy to the load. The MPPT function will regulate the each input at different optimal operating points which requires fast convergence, accurate regulation and good stability. No dependency is allowed among all inputs for accurate MPPT performance especially in irradiation fast changing condition. In order to minimize the components in the DC-DC converter, an inductor sharing scheme is applied in this multi-input energy harvesting system [49]. The single inductor has been time shared by all multi-junction PVs to maintain Boost converter switch operation. All inputs are connected to the Boost converter in an interleaved way.

Within each selected window, the shared inductor will be energized and de-energized through the high side switches.

The converter can operate in either continuous conduction mode (CCM) or discontinuous conduction mode (DCM). If the converter works at steady state in CCM condition, the average current will be maintained constant while the valley will vary according to the different duty cycle, input and output, which makes the starting point of next cycle dependent on the previous cycle. Therefore, the DCM operation is perfect for single inductor time sharing structure. As shown on the diagram in Figure 17, when the inductor current of one sub-converter reduces to zero, another sub-converter is turned on, which leads to the varying frequency in different conditions. Varying frequency creates more freedom to modulate the PV current, which also regulates the PV voltage in an inverse way. The total conduction time is determined by the inductor current.

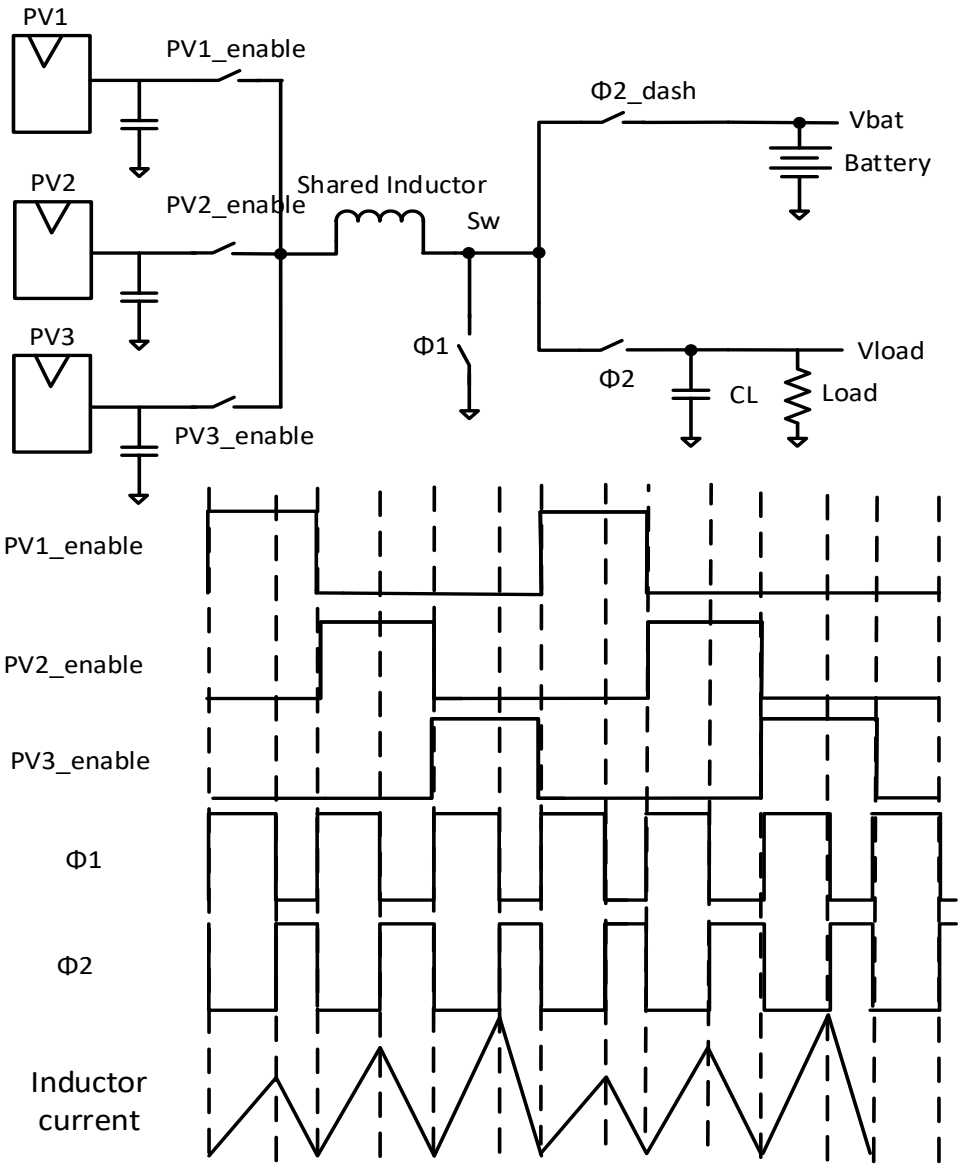

Figure 17. DCM Inductor Current Sharing

By invoking voltage-second balance, we have the turn on and turn off time relationship for each input as below:

$$t_2 = t_1 \frac{V_{PV1}}{V_{OUT} - V_{PV1}}$$

Thus the input impedance can be obtained as

$$\bar{Z}_{in1} = \frac{V_{PV1}}{\bar{I}_{in1}} = 2L * (\frac{1}{t_1} + \frac{V_{OUT} - V_{PV1}}{V_{OUT} - V_{PV2}} * \frac{t_3}{{t_1}^2})$$

By utilizing Boost converter, the output over input voltage ratio is ensured as high. So $\frac{V_{OUT}-V_{PV1}}{V_{OUT}-V_{PV2}}$ can be seen as almost constant in steady state. While $\frac{t_3}{{t_1}^2}$ is strongly dependent on t_1, which is generated by the loop controller. Thus, the sub-converter can be tuned as the load of the input PV for impedance matching to extract optimal MPP out of each PV junction.

To achieve the multi-input sharing, one finite state machine is defined as below algorithm in Figure 18. The input phase switching will be triggered by the rising edge of high side switch discharge pulse width t_{off} when the inductor current reduces to zero, which also ensures the DCM operation. Thus, the interleaved operation for multi-junction PV is ensured by the embedded finite state machine.

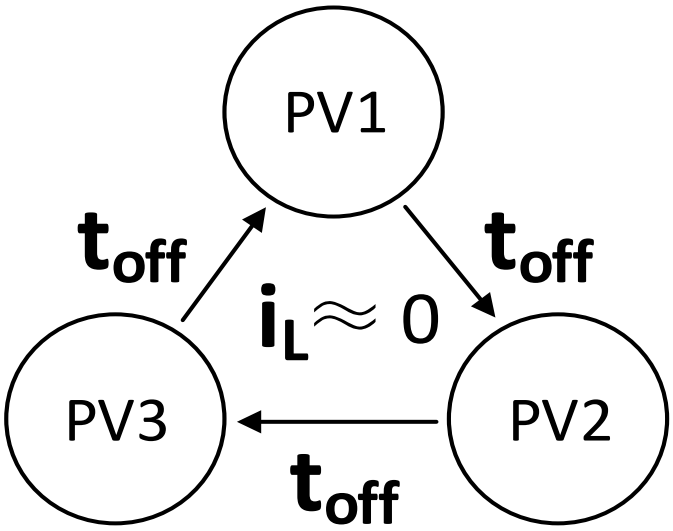

Figure 18. Input Phase Switching Algorithm

3.4 Dual-path Output regulation

Limited by the maximum PV current, the load command is usually less than PV maximum power. Therefore, most of the MPPT circuit will push the PV out of the MPP

condition at light load condition, which leads to an energy waste. By introducing the battery as a second output path, the extra energy can be stored at light load condition. Furthermore, as shown in Figure 19, by sensing the feedback output voltage and comparing with the reference voltage, the Dual-path regulator block will decide in which path the inductor need to charge during the de-energizing phase. Compared with traditional two stage design, by reusing the MPPT stage Boost converter, regulated output voltage is obtained at 3V without one more stage power loss.

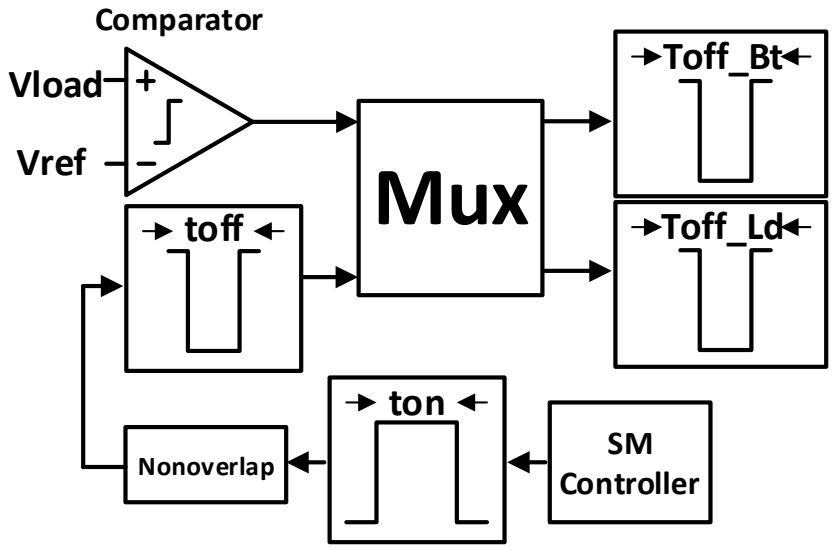

Figure 19. Dual-path Output Regulator

CHAPTER 4

STABILITY ANALYSIS AND LOOP CONTROL

4.1 Inductor Current Based Control

As shown in the Figure 20, the inductor current based control topology is applied in this work. At the output node of PV, the PV current, input capacitor current and inductor current hold Kirchhoff current law:

$$i_{\mathrm{PV}} = i_{\mathrm{CAP}} + i_{\mathrm{L}}$$

The negative feedback in the current controller loop will clamp the inductor current to i_{REF} in steady-state, While i_{REF} is the output of the compensator as the reference of the inductor current.

$$i_{\mathrm{e}} = i_{\mathrm{REF}} - i_{\mathrm{L}}$$

$$i_{\mathrm{PV}} = i_{\mathrm{CAP}} + i_{\mathrm{REF}} - i_{\mathrm{e}}$$

Where the capacitor current and error current are both zero in steady-state, which leads to

$$i_{\mathrm{PV}} = i_{\mathrm{REF}}$$

Therefore, by regulating the inductor current, the PV current is regulated accordingly. The current reference i_{REF} will be generated by the feedback loop to minimize the voltage error between PV voltage and the reference voltage from the P&O loop. As long as the inner loop is fast enough, i_{PV} can be regulated even in prompt irradiation changing condition to extract the maximum power.

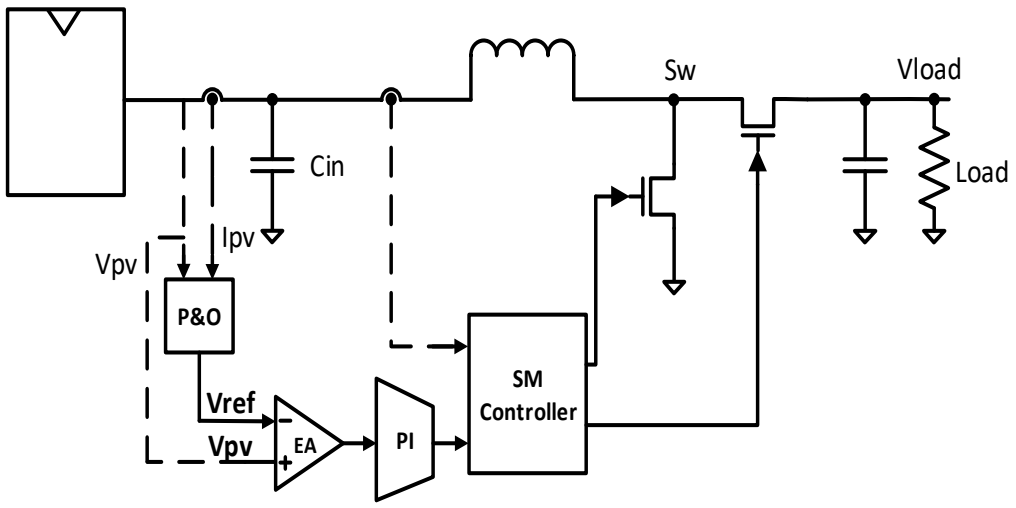

Figure 20. Inductor Current Based Control Loop

4.2 Sliding-Mode MPPT

The classic MPPT algorithm is designed based on constant irradiation. The P&O method is largely used in MPPT application to dynamically track the maximum power point in changing illumination condition. However, by perturbing the small change in voltage, the algorithm seeks the right direction to achieve the peak power point by power comparison. Therefore, the P&O performance is significantly depending on the perturbation step size and frequency [45]. The optimal MPP performance is ensured by selecting the minimum step size in steady state, which leads to the penalty of losing speed in the abrupt transient change in the sunlight. The larger the irradiation is changed the bigger step we need to achieve high MPP efficiency. Just as P&O, most of the algorithms in MPPT research is voltage based because of the fine correlation dependence of the voltage step around MPP compared with the current. While, the linear dependence of the PV current on the irradiation level can benefit the re-tracking speed. Thus, by utilizing the dual-loop control, we can have the accurate control ability around the optimal power from outer voltage loop

as well as the fast transient response in big irradiation changing condition from the inner current loop. As mentioned above, the regulating target is $i_{\mathrm{PV}} = i_{\mathrm{REF}}$. To utilize the sliding-mode control, we set the sliding surface as

$$\Psi = i_{\mathrm{PV}} - i_{\mathrm{REF}}$$

The reference current i_{REF} is determined by the compensator output. Once the system works in sliding-mode, the surface Ψ will be converged into zero. Any deviation of the sliding surface away from the zero state will be rejected, resulting from the PV voltage V_{PV} locking at P&O outer loop reference voltage V_{REF}. The strong current control capability rejects the PV voltage perturbation in prompt irradiation change condition as well as keeps PV current i_{PV} tracking irradiation level.

To hold the sliding mode operation, two key requirements need to be fulfilled:

$$\Psi = 0$$

$$\frac{d\Psi}{dt} = 0$$

In the Boost converter, by turning on and off the switches, the converter is modulated. The unified equation for inductor current in the switching state is

$$\frac{di_{\mathrm{L}}}{dt} = \frac{V_{\mathrm{PV}} - (1-u) * V_{\mathrm{OUT}}}{L}$$

Where u is the variable determining the switch state. $u = 1$ when low side switch is on while $u = 0$ at switch off state. Since the sliding surface equation can be simplified as below

$$\frac{d\Psi}{dt} = \frac{di_{\mathrm{L}}}{dt} - \frac{di_{\mathrm{REF}}}{dt}$$

Thus

$$\frac{d\Psi}{dt} = \frac{V_{\mathrm{PV}} - (1-u) * V_{\mathrm{OUT}}}{L} - \frac{di_{\mathrm{REF}}}{dt}$$

The inductor current keeps increasing when low side switch is on, which leads to the sliding surface moving to the positive direction. And the inductor current keeps decreasing when the low side switch is off, which turns the sliding surface into negative direction instead. In conclusion, by switching operation, the sliding surface can be modulated around zero.

$$\text{when } \Psi < 0 \text{ low side switch turns on}$$

$$\text{when } \Psi > 0 \text{ low side switch turns off}$$

4.3 Loop stability and Compensation

By using the sliding mode control technique, the Boost converter is utilized as a tunable current source. The whole Boost converter is modulated to regulate the PV voltage. In ac stability angle, it equals to adjusting the capacitor current to modulate the shunt capacitor voltage.

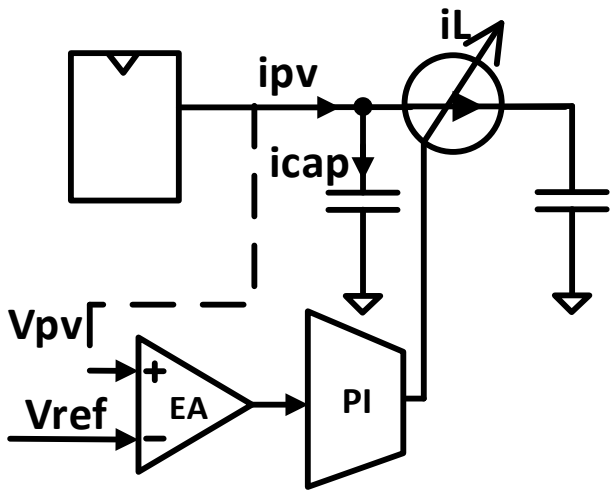

Figure 21. AC Loop Stability

Thus, as shown in Figure 21, when we close the loop at the input capacitor, the

modulation relationship between reference current to PV voltage can be simplified as below

$$\mathrm{H}_{\frac{v}{i}}(\mathrm{s}) = -\frac{1}{c_{in} * s}$$

Resulting from the inner current mode control, the classic two poles system for the Boost converter can be simplified as one pole system instead. Therefore, in this work, a traditional PI compensator is applied to achieve enough phase margin.

The PI compensator transfer function is shown as below

$$G_{comp}(\mathrm{s}) = \mathrm{k}_p + \frac{\mathrm{k}_i}{s}$$

The total transfer function of the whole loop

$$H_{CL} = G_{comp}(\mathrm{s}) * \mathrm{H}_{\frac{v}{i}}(\mathrm{s})$$

After selecting proper settling time to ensure the system function in the fastest P&O loop frequency condition, the PI compensator is obtained by the MATLAB loop analysis tools.

4.4 Current Controller Sharing

The complementary pulse width signals are generated as the output of the sliding mode controller. However, all multi-junction PVs need to be regulated simultaneously via one adjustable inductor current from the Boost converter. So the duty cycle signal will be shared among all inputs. In additional, the sliding mode controller need to be shared among all compensators. The loop diagram is as shown in Figure 22.

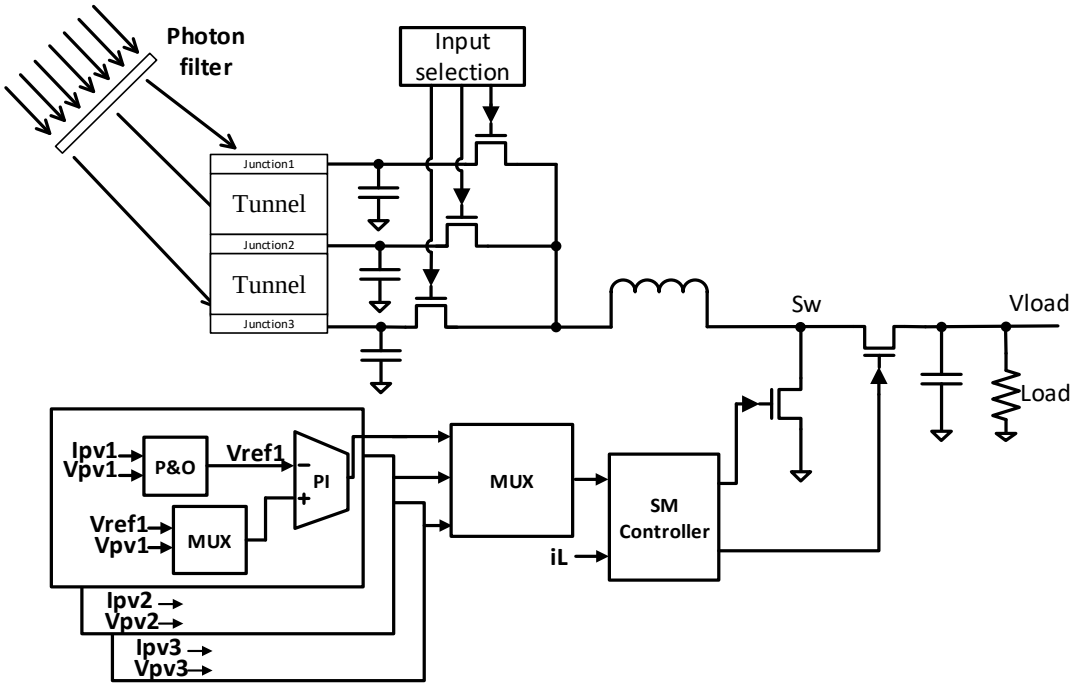

Figure 22. Inner Current Control Sharing

CHAPTER 5

EXPERIMENTAL RESULTS

The proposed system has been implemented and measured in the PCB platform. As shown in the Fig. 23, the PV was integrated on the board. By stacking the standard PV bits with double and triple fashion, three gap material based multi-junction PV was mimicked. The new PV parameters have been characterized in the lab with PV tracer as shown in Table 1.

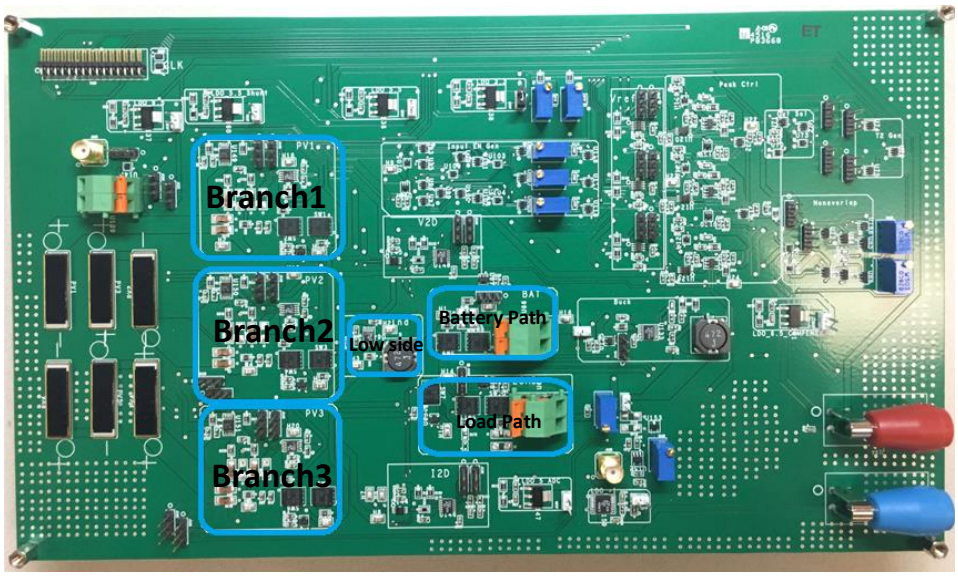

Figure 23. Board picture

Table 1: Parameters of PV Inputs

	PV1	PV2	PV3
Short-circuit I_{STC} (mA)	50	48	46
Open-circuit V_{OC} (mV)	500	940	1450
MPP current Impp (mA)	44.6	43	42
MPP voltage Impp (mV)	390	780	1100
Maximum Power (mW)	17.4	33.5	46.2

Figure 24 shows that the inductor current operated in DCM with alternate input sources. During each selected input phase, the inductor current was energized by different input source independently without reverse current or big ringing at the switching node. The input sharing phases were not identical because the duration was determined by the different input voltage level and different peak current level. The DCM operation was maintained by the cycle by cycle peak current mode control benefiting from the inner sliding mode current controller.

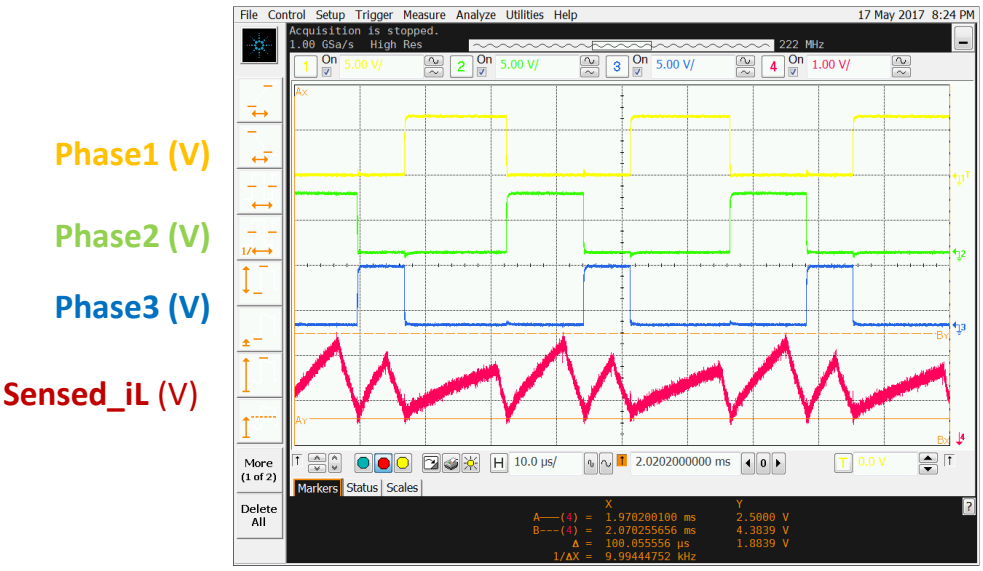

Figure 24. Inductor Sharing DCM Operation

As is discussed above, the input was regulated by feeding the sensed input voltage to the error amplifier. And the inner sliding mode current controller was shared by three compensation blocks. The compensation block for each input was only selected through mux during its conduct phase. The mux output was connected to the inner current controller. Furthermore, the compensation block was held during the idle time when the other phases were selected, which led to a smooth input voltage regulation during the input switch transition.

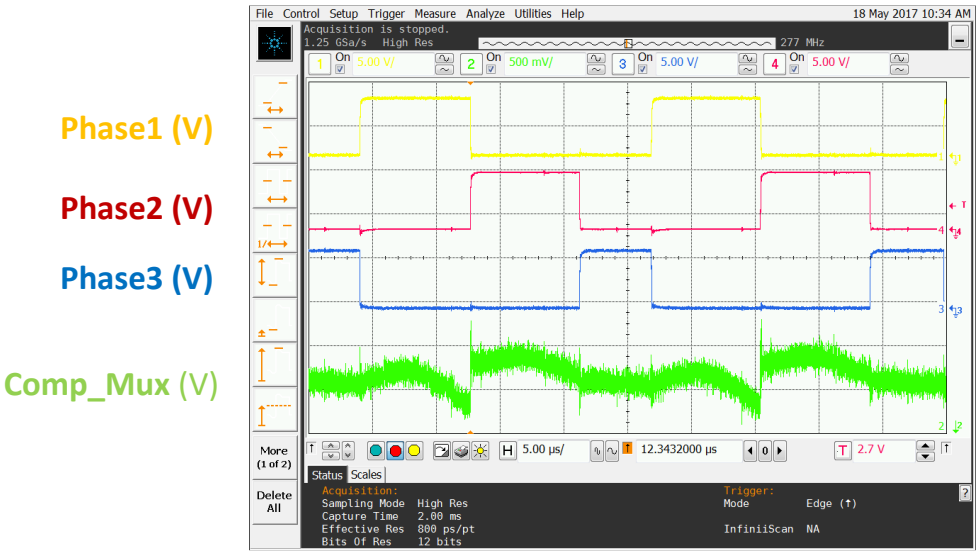

Figure 25. Compensation Mux Out

Thus, the input regulation was achieved by the dual-loop control. The outer P&O loop dynamically generated an optimal voltage reference for the inner loop. The three-level toggle behavior showed that the maximum power point was achieved by outer loop. And the inner sliding mode current loop accurately controlled the inductor current cycle by cycle. All inputs were regulated around the MPP condition as Figure 26 – 28. PV1, PV2 and PV3 were regulated around 388, 784 and 1100 mV.

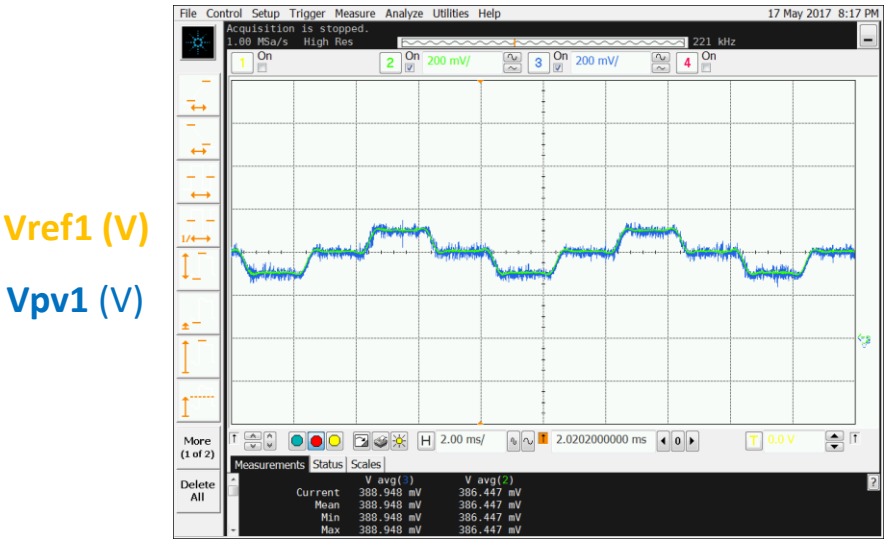

Figure 26. PV1 MPP Regulation

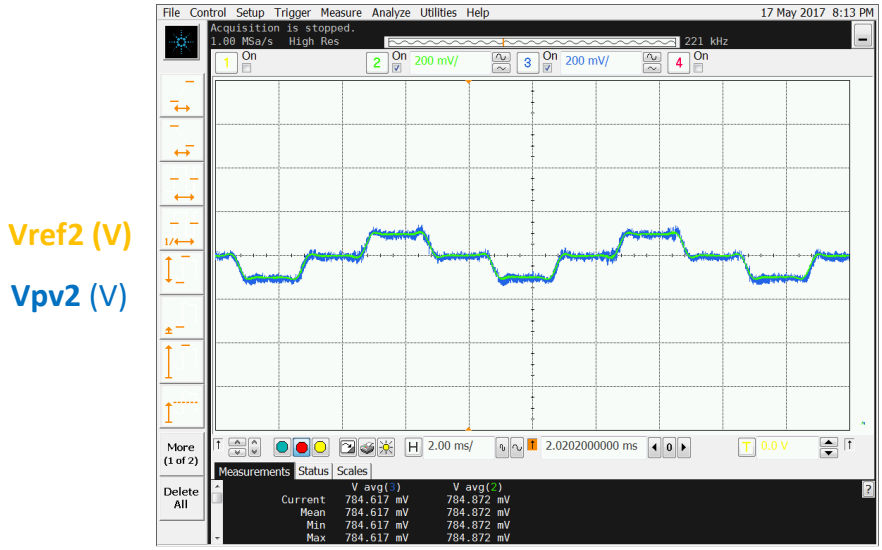

Figure 27. PV2 MPP Regulation

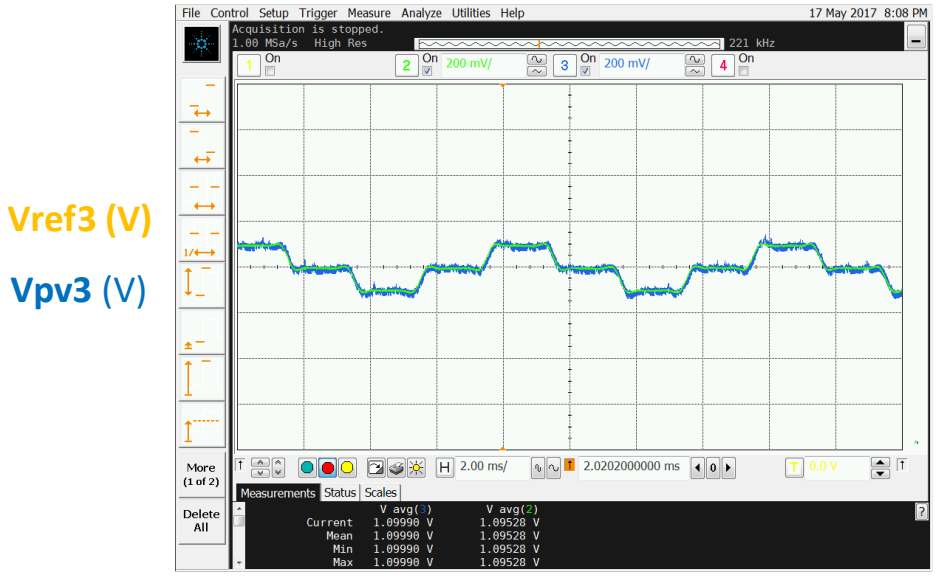

Figure 28. PV3 MPP Regulation

The output voltage regulation is a fundamental requirement for power management. The output capacitor held the output during the inductor rising period. And during the inductor deenergizing phase, the output voltage rose till the idle time. By reusing the MPPT single stage Boost, regulated output voltage was obtained around 3V with voltage ripple of 80mV, as shown in Figure 29 -30. The output ripple can easily be improved by increasing the output capacitor value which is not our focus here.

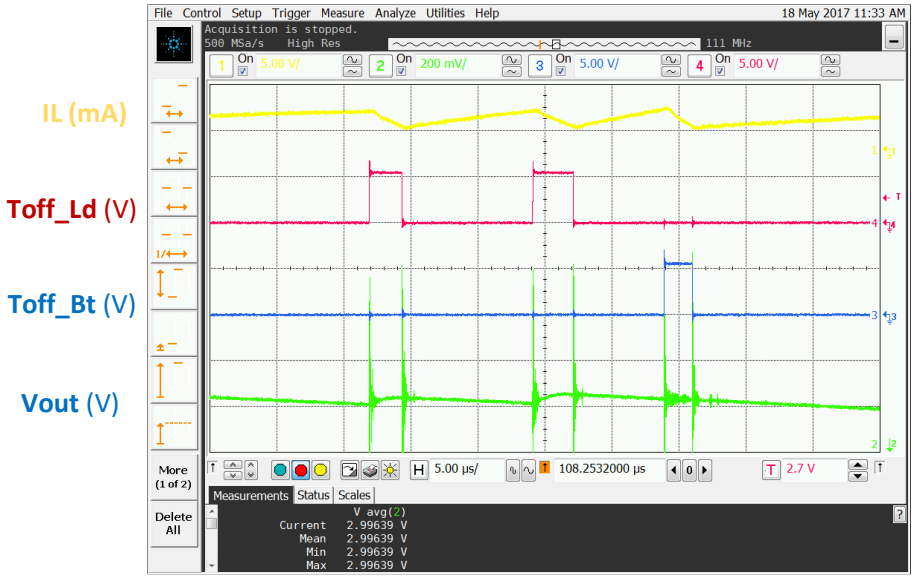

Figure 29. Dual-path Output Voltage Regulation

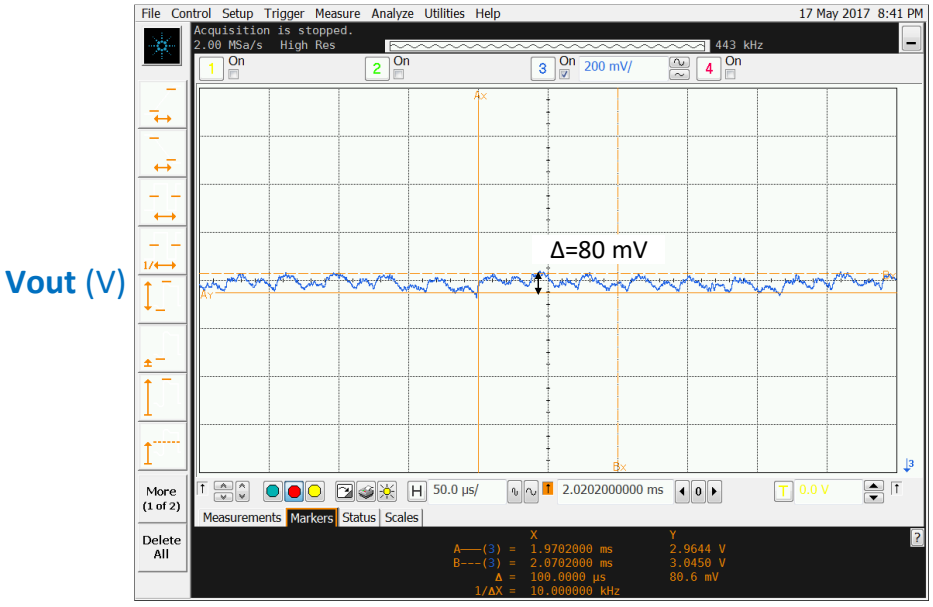

Figure 30. Output Voltage Ripple

Due to the linear dependency of the PV current on the sunlight illumination density, the maximum power need to be re-tracked dynamically in real life. Figure 31 shows the re-tracking behavior of this system when the sunlight changes abruptly. Figure 32 shows the

response time measurement result when we zoom in the plot. In this test case, the system recovered from the Voc condition which is the worst condition. The system could be re-tracked back to MPP condition within 82us. Compared with the typical PWM based MPPT system, the proposed system has a much fast response behavior.

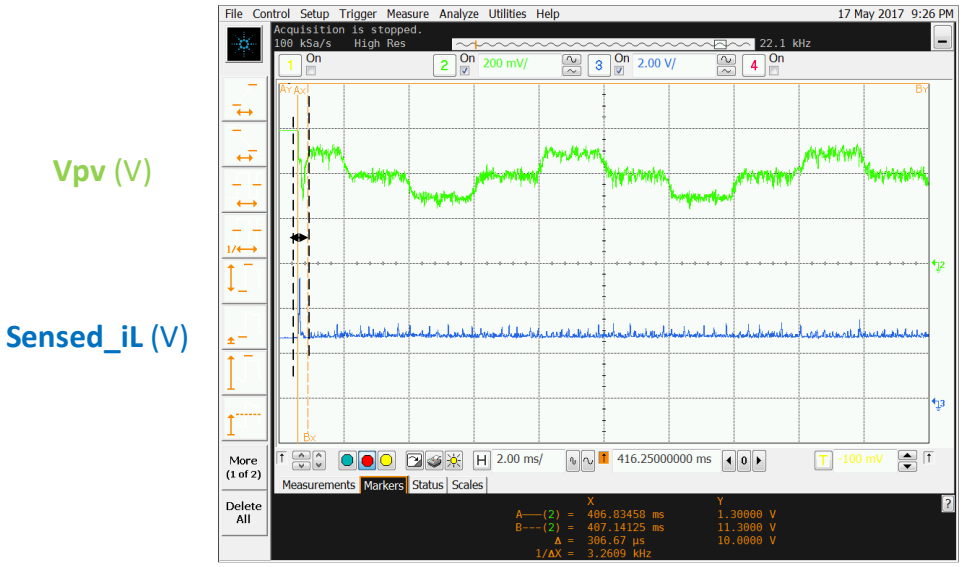

Figure 31. Transient Response Behavior

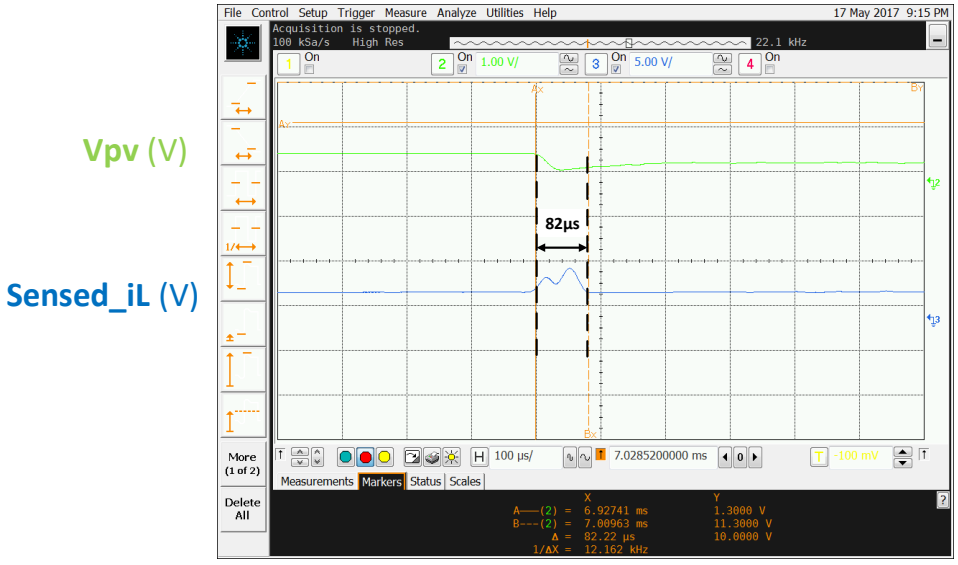

Figure 32. Zoom in Response Time Measurement

CHAPTER 6

CONCLUSION AND FUTURE WORK

This thesis proposes Multi-input single inductor Dual-output Boost based architecture for Multi-junction PV energy harvesting source. The system works in Discontinuous Conduction Mode to achieve the independent input regulation for multi-junction PV source. Inductor sharing provides a single stage platform for combining power from MJ-PV sub-cells. The input PV cells provide a few hundred milli-watt of power. A dual-output path is implemented to regulate the output at 3.3 V as well as store the extra energy at light load condition. The dual-loop based sliding-mode MPPT for multi-junction PV is proposed to speed up the system response time for prompt irradiation change as well as maximize MPPT efficiency. The boost converter works at around 300K Hz and each input is regulated at around 100K Hz. The measured peak efficiency is 83% and MPPT efficiency is 95%.

The future work includes the following:

1) Instead of using one dimensional sliding surface, a tunable sliding surface can be added to speed up the transient performance in voltage.

2) The energy stored in the battery can be recycled by reusing the single stage DC-DC instead of using Buck converter as an independent path.

3) The DCM operation can be extended into Pseudo Continuous Conduction Mode, which leads to less ripple in heavy input power condition. This can be tested in the existing system by changing the valley reference value without any other modification.

REFERENCES

[1] R. S. Ohl, “Light sensitive electric device,” U.S. Patent 2402662, Jun. 1946.

[2] R. S. Ohl, “Light sensitive electric device including silicon,” U.S. Patent 443542, Jun. 1948.

[3] J. Zhao, A. Wang, and M. A. Green, “24.5% efficiency silicon PERT cells on MCZ substrates and 24.7% efficiency PERL cells on FZ substrates,” Prog. Photovolt.: Res. Appl., vol. 7, no. 6, pp. 471–474, 1999.

[4] D. M. Chapin, C. S. Fuller, and G. L. Pearson, “A new silicon p-n junction photocell for converting solar radiation into electrical power,” J. Appl. Phys., vol. 25, no. 5, pp. 676–677, 1954.

[5] T. Torfs et al., “Wearable autonomous wireless electro-encephalography system fully powered by human body heat,” in Proc. IEEE Sensors, Oct. 2008, pp. 1269–1272.

[6] A. Luque and A. Mart´ı, “Theoretical limits of photovoltaic conversion,” in Handbook of Photovoltaic Science and Engineering, A. Luque and S. Hegedus, Eds. Chicester, U.K.: Wiley, 2011.

[7] D. J. Friedman, “Progress and challenges for next-generation high-efficiency multijunction solar cells,” Curr. Opin. Solid St. M. 14(6), 131–138 (2010).

[8] H. Lhermet, C. Condemine, M. Plissonnier, R. Salot, P. Audebert, and M. Rosset, “Efficient power management circuit: From thermal energy harvesting to above-IC microbattery energy storage,” IEEE J. Solid-State Circuits, vol. 43, no. 1, pp. 246–255, Jan. 2008.

[9] “Solar Super Cells,” [Online]. Available: http://www.solarmade.com/

[10] Saurav Bandyopadhyay, Anantha P. Chandrakasan, “Platform Architecture for Solar, Thermal, and Vibration Energy Combining With MPPT and Single Inductor,” IEEE J. Solid-State Circuits, vol. 47, no. 9, pp. 2199–2215, Sep. 2012.

[11] Y. Jiang, J.A. Abu Qahouq, “Single-sensor multi-channel maximum power point tracking controller for photovoltaic solar systems,” IET Power Electron., Vol. 5, Iss. 8, pp. 1581–1592, Aug. 2012.

[12] Cheng-Yu Tang, Yao-Ting Chen, Yaow-Ming Chen, “PV Power System With Multi-Mode Operation and Low-Voltage Ride-Through Capability,” IEEE Transactions On Industrial Electronics, vol. 62, no. 12, pp. 7524-7533, Dec. 2015.

[13] Il-Song Kim, Myung-Bok Kim, Myung-Joong Youn, “New Maximum Power Point Tracker Using Sliding-Mode Observer for Estimation of Solar Array Current in the Grid-Connected Photovoltaic System,” IEEE Transactions On Industrial Electronics, vol. 53, no. 4, pp.1027-1035, Aug. 2006.

[14] Daniel Gonz´alez Montoya, Carlos Andr´es Ramos-Paja, Roberto Giral, “Improved Design of Sliding-Mode Controllers Based on the Requirements of MPPT Techniques,” IEEE Transactions On Power Electronics, vol. 31, no. 1, pp.235-247, Jan. 2016.

[15] Reham Haroun, Abdelali El Aroudi, Angel Cid-Pastor, Germain Garcia, Carlos Olalla, Luis Mart´ınez-Salamero, “Impedance Matching in Photovoltaic Systems Using Cascaded Boost Converters and Sliding-Mode Control,” IEEE Transactions On Power Electronics, vol. 30, no. 6, pp. 3185-3199, June 2015.

[16] Emilio Mamarelis, Giovanni Petrone, Giovanni Spagnuolo, “Design of a Sliding-Mode-Controlled SEPIC for PV MPPT Applications,” IEEE Transactions On Industrial Electronics, vol. 61, no. 7, pp. 3387-3398, JULY 2014.

[17] Yoash Levron, Doron Shmilovitz, “Maximum Power Point Tracking Employing Sliding Mode Control,” IEEE Transactions On Circuits And Systems—I: Regular Papers, vol. 60, no. 3, pp.724-732, Mar. 2013.

[18] Enrico Bianconi, Javier Calvente, Roberto Giral, Emilio Mamarelis, Giovanni Petrone, etc., “A Fast Current-Based MPPT Technique Employing Sliding Mode Control reference,” IEEE Transactions on Industrial Electronics, vol. 60, no. 3, pp. 1168-1178, March 2013.

[19] A. S. Sedra and K. C. Smith, Microelectronic Circuits. London, U.K.: Oxford Univ. Press, 2006.

[20] H. J. Moller, ¨ Semiconductors for Solar Cells. Norwood, MA: Artech House, 1993.

[21] A. L. Fahrenbruch and R. H. Bube, Fundamentals of Solar Cells. San Francisco, CA: Academic, 1983.

[22] F. Lasnier and T. G. Ang, Photovoltaic Engineering Handbook. New York: Adam Hilger, 1990.

[23] H. S. Rauschenbach, Solar Cell Array Design Handbook. New York: Van Nostrand Reinhold, 1980.

[24] L. L. Buciarelli, B. L. Grossman, E. F. Lyon, and N. E. Rasmussen, “The energy balance associated with the use of a MPPT in a 100 kW peak power system,” in IEEE Photovoltaic Spec. Conf., 1980, pp. 523–527.

[25] J. D. van Wyk and J. H. R. Enslin, “A study of wind power converter with microprocessor based power control utilizing an oversynchronous electronic scherbius cascade,” in Proc. IEEE Int. Power Electron. Conf., 1983, pp. 766–777.

[26] W. J. A. Teulings, J. C. Marpinard, A. Capel, and D. O’Sullivan, “A new maximum power point tracking system,” in Proc. 24th Annu. IEEE Power Electron. Spec. Conf., 1993, pp. 833–838.

[27] Y. Kim, H. Jo, and D. Kim, “A new peak power tracker for cost-effective photovoltaic power system,” in Proc. 31st Intersociety Energy Convers. Eng. Conf., 1996, pp. 1673–1678.

[28] O. Hashimoto, T. Shimizu, and G. Kimura, “A novel high performance utility interactive photovoltaic inverter system,” in Conf. Record 2000 IEEE Ind. Applicat. Conf., 2000, pp. 2255–2260.

[29] E. Koutroulis, K. Kalaitzakis, and N. C. Voulgaris, “Development of a microcontroller-based, photovoltaic maximum power point tracking control system,” IEEE Trans. Power Electron., vol. 16, no. 21, pp. 46–54, Jan. 2001.

[30] M. Veerachary, T. Senjyu, and K. Uezato, “Maximum power point tracking control of IDB converter supplied PV system,” in IEE Proc. Elect. Power Applicat., 2001, pp. 494–502.

[31] W. Xiao and W. G. Dunford, “A modified adaptive hill climbing MPPT method for photovoltaic power systems,” in Proc. 35th Annu. IEEE Power Electron. Spec. Conf., 2004, pp. 1957–1963.

[32] O. Wasynczuk, “Dynamic behavior of a class of photovoltaic power systems,” IEEE Trans. Power App. Syst., vol. 102, no. 9, pp. 3031–3037, Sep. 1983.

[33] C. Hua and J. R. Lin, “DSP-based controller application in battery storage of photovoltaic system,” in Proc. IEEE IECON 22nd Int. Conf. Ind. Electron., Contr. Instrum., 1996, pp. 1705–1710.

[34] M. A. Slonim and L. M. Rahovich, “Maximum power point regulator for 4 kW solar cell array connected through invertor to the AC grid,” in Proc. 31st Intersociety Energy Conver. Eng. Conf., 1996, pp. 1669–1672.

[35] A. Al-Amoudi and L. Zhang, “Optimal control of a grid-connected PV system for maximum power point tracking and unity power factor,” in Proc. Seventh Int. Conf. Power Electron. Variable Speed Drives, 1998, pp. 80–85.

[36] N. Kasa, T. Iida, and H. Iwamoto, “Maximum power point tracking with capacitor identifier for photovoltaic power system,” in Proc. Eighth Int. Conf. Power Electron. Variable Speed Drives, 2000, pp. 130–135.

[37] L. Zhang, A. Al-Amoudi, and Y. Bai, “Real-time maximum power point tracking for grid-connected photovoltaic systems,” in Proc. Eighth Int. Conf. Power Electronics Variable Speed Drives, 2000, pp. 124–129.

[38] C.-C. Hua and J.-R. Lin, “Fully digital control of distributed photovoltaic power systems,” in Proc. IEEE Int. Symp. Ind. Electron., 2001, pp. 1–6.

[39] M.-L. Chiang, C.-C. Hua, and J.-R. Lin, “Direct power control for distributed PV power system,” in Proc. Power Convers. Conf., 2002, pp. 311– 315.

[40] K. Chomsuwan, P. Prisuwanna, and V. Monyakul, “Photovoltaic gridconnected inverter using two-switch buck-boost converter,” in Conf. Record Twenty-Ninth IEEE Photovoltaic Spec. Conf., 2002, pp. 1527–1530.

[41] Y.-T. Hsiao and C.-H. Chen, “Maximum power tracking for photovoltaic power system,” in Conf. Record 37th IAS Annu. Meeting Ind. Appl. Conf., 2002, pp. 1035–1040.

[42] Y. Jung, G. Yu, J. Choi, and J. Choi, “High-frequency DC link inverter for grid-connected photovoltaic system,” in Conf. Record Twenty-Ninth IEEE Photovoltaic Spec. Conf., 2002, pp. 1410–1413.

[43] S. Jain and V. Agarwal, “A new algorithm for rapid tracking of approximate maximum power point in photovoltaic systems,” IEEE Power Electron. Lett., vol. 2, no. 1, pp. 16–19, Mar. 2004.

[44] T. Tafticht and K. Agbossou, “Development of a MPPT method for photovoltaic systems,” in Canadian Conf. Elect. Comput. Eng., 2004, pp. 1123–1126.

[45] N. Femia, G. Petrone, G. Spagnuolo, and M. Vitelli, “Optimization of perturb and observe maximum power point tracking method,” IEEE Trans. Power Electron., vol. 20, no. 4, pp. 963–973, Jul. 2005.

[46] P. J. Wolfs and L. Tang, “A single cell maximum power point tracking converter without a current sensor for high performance vehicle solar arrays,” in Proc. 36th Annu. IEEE Power Electron. Spec. Conf., 2005, pp. 165–171.

[47] N. S. D’Souza, L. A. C. Lopes, and X. Liu, “An intelligent maximum power point tracker using peak current control,” in Proc. 36th Annu. IEEE Power Electron. Spec. Conf., 2005, pp. 172–177.

[48] N. Kasa, T. Iida, and L. Chen, “Flyback inverter controlled by sensorless current MPPT for photovoltaic power system,” IEEE Trans. Ind. Electron., vol. 52, no. 4, pp. 1145–1152, Aug. 2005.

[49] Y. K. Ramadass and A. P. Chandrakasan, “An efficient piezoelectric energy harvesting interface circuit using a bias-flip rectifier and shared inductor,” IEEE J. Solid-State Circuits, vol. 45, no. 1, pp. 189–204, Jan. 2010.